Geophysical Research Letters

RESEARCH LETTER
10.1029/2020GL087908

Radiocarbon Dating of Silica Sinter and Postglacial Hydrothermal Activity in the El Tatio Geyser Field

Carolina Munoz-Saez[1,2], Michael Manga[3], Shaul Hurwitz[4], Silvina Slagter[1,2,5], Dakota M. Churchill[3], Martin Reich[1,2], David Damby[4], and Diego Morata[1,2]

[1]Department of Geology and Andean Geothermal Center of Excellence (CEGA), FCFM, Universidad de Chile, Santiago, Chile, [2]Millennium Nucleus for Metal Tracing Along Subduction, FCFM, Universidad de Chile, Santiago, Chile, [3]Department of Earth and Planetary Science, University of California, Berkeley, CA, USA, [4]U.S. Geological Survey, Moffett Field, CA, USA, [5]Department of Geology and Geophysics, Yale University, New Haven, CT, USA

Key Points:
- El Tatio is a long-lived hydrothermal system, active for at least 27 ka
- Dated sinter deposits provide bounds on recent volcanic activity and deglaciation in the vicinity of El Tatio
- Bacterial mats trapped in sinter lead to old apparent radiocarbon ages

Supporting Information:
- Supporting Information S1
- Table S1

Correspondence to:
C. Munoz-Saez,
caromuno@ing.uchile.cl

Citation:
Munoz-Saez, C., Manga, M., Hurwitz, S., Slagter, S., Churchill, D. M., Reich, M., et al. (2020). Radiocarbon dating of silica sinter and postglacial hydrothermal activity in the El Tatio geyser field. *Geophysical Research Letters*, *47*, e2020GL087908. https://doi.org/10.1029/2020GL087908

Received 12 MAR 2020
Accepted 22 MAY 2020
Accepted article online 30 MAY 2020

Abstract The El Tatio geothermal field in the Chilean Altiplano contains hydrothermal silica sinter deposits overlaying glacial and volcanic units, providing an opportunity to constrain the timing of deglaciation and volcanic activity in an area with sparse absolute chronologies. We obtained 51 new radiocarbon ages and $\delta^{13}C$ values on the organic material trapped in these sinter deposits. Based on the $\delta^{13}C$ values, we exclude 29 samples for possible contamination with bacterial mats that incorporate old carbon. We infer that hydrothermal activity initiated ~27 ka ago and has been nearly continuous ever since. The ages of the oldest sinter deposits coincide with ages of moraines that stabilized after the most recent deglaciation. Whereas late Pleistocene sinters are broadly distributed in the field, Holocene deposits are found around active hydrothermal features. Although recent volcanism is absent in the vicinity of El Tatio, persistent hydrothermal discharge implies a long-lived magmatic heat source.

Plain Language Summary The El Tatio geothermal field in the Chilean Altiplano contains large deposits of silica precipitated by hot springs, called sinter or geyserite. Silica sinter traps organic material that is suitable for radiocarbon dating; however, previous attempts using this methodology have shown inconsistencies that still need to be critically assessed. Here, we found that bacteria can contaminate the radiocarbon measurements leading to older radiocarbon ages. Stable carbon isotopes (^{13}C and ^{12}C) in dated material can be used to evaluate when the organic matter is contaminated and thus provides an unreliable age. Sinter deposits in El Tatio overlay glacial deposits and volcanic units; thus, sinter ages provide a bound for volcanism and deglaciation in the area. Uncontaminated radiocarbon ages indicate that El Tatio is a long-lived geothermal system that started at least ~27 ka ago and has been active since. However, the spatial distribution of thermal water discharge in the field has changed over time. The onset of hydrothermal activity is consistent with the onset of deglaciation in the Chilean Altiplano. Even though recent volcanic deposits are absent in the vicinity of El Tatio, the persistent discharge of hot water implies a significant long-lived magmatic source providing heat to the geothermal system.

1. Introduction

The El Tatio geothermal field in Northern Chile (~22°20′S, ~4,300 m above sea level, Figure 1), one of the largest geothermal fields in South America, is a near-surface manifestation of the Altiplano-Puna Volcanic Complex (e.g., De Silva, 1989; Salisbury et al., 2011). Based on the current rates of silica precipitation and the thickness of the sinter deposits in El Tatio, Nicolau et al. (2014) inferred that deposition would likely have begun at ~4 ka. However, radiocarbon ages of sinter deposits from the active hydrothermal area yielded ages up to 10.8 ka BP (Slagter et al., 2019). Holocene sinters overlie older sinter platforms that extend beyond the active hydrothermal area, suggesting an even earlier inception of hydrothermal activity (Figure 1 and supporting information Figures S1 and S2). Sinter deposits also overlay volcanic and glacial units of Pleistocene or Holocene ages based on stratigraphic relationships (e.g., Lahsen, 1976; Marinovic & Lahsen, 1984). Determining the age and mineralogy of hydrothermal deposits provides an opportunity to set bounds for the Quaternary volcanic and glacial activity in an area with sparse and highly scattered chronologies (e.g., Ward et al., 2015, 2017).

Sinter deposits are commonly found in areas with near-neutral to alkali chloride hot springs and originate from subsurface reservoirs with temperatures >175°C (e.g., Fournier, 1977; Giggenbach, 1988). Different

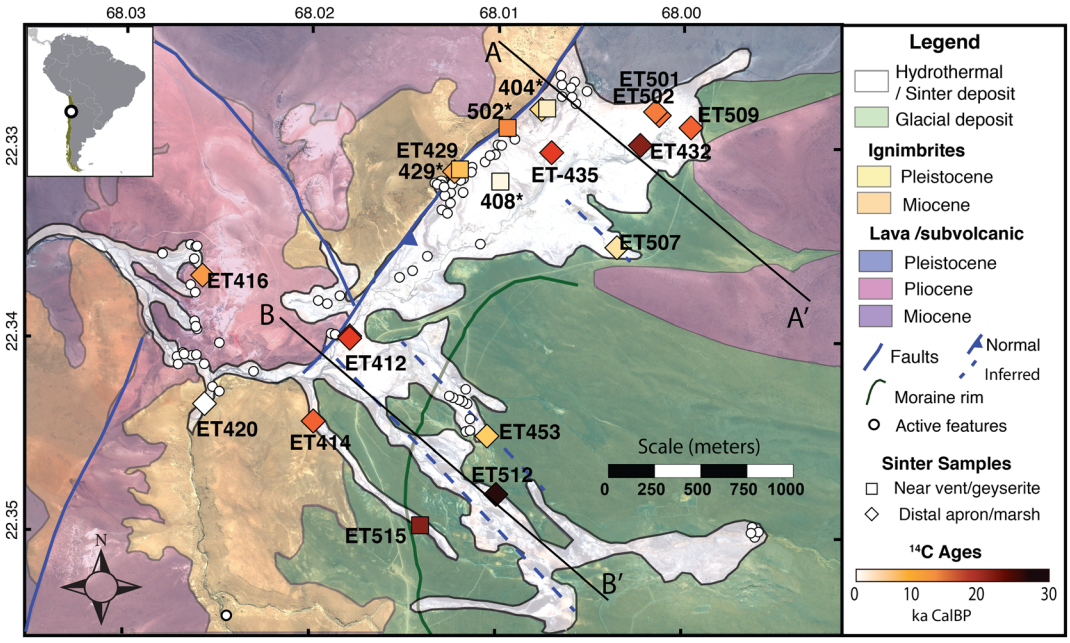

Figure 1. Geology of El Tatio geothermal field (Lahsen, 1976; Marinovic & Lahsen, 1984). Shape of the symbols indicates the depositional environment, and color (color bar) shows reliable ages. For samples with duplicates, we calculated the weighted mean (Table S1). Samples labeled ET belong to this study, while samples with asterisks are from Slagter et al. (2019).

assemblages of microorganisms and macroorganisms inhabit sinter deposits depending on temperature, pH, and hydrodynamics (e.g., Campbell et al., 2015; Jones & Renaut, 2003; Konhauser et al., 2003). Silica precipitates from cooling and evaporating water as amorphous opal-A and over time matures to opal-CT, opal-C, and finally quartz in ~50 ka, providing a relative age for the sinter deposits (Herdianita et al., 2000; Rodgers et al., 2004). However, the rate of silica maturation in sinter depends on postdepositional environmental conditions such as the presence of organic matter, carbonate minerals, weathering, or acidic fluid condensate (e.g., Campbell et al., 2003, 2015; Jones & Renaut, 2003; Lynne et al., 2005, 2007; Rodgers et al., 2004) Those postdepositional environmental conditions can vary across the hydrothermal field, thus determining sinter ages based on mineralogy can only be applied within a thermal area if the stratigraphy of the deposits is constrained.

Midtemperature to low-temperature environments host and preserve a large diversity of organic materials trapped in the sinter deposits, including remains of plants and animals (e.g., Campbell et al., 2015; Jones & Renaut, 2003). Radiocarbon dating has been applied to silica sinter deposits from many active geothermal areas worldwide (e.g., Drake et al., 2014; Howald et al., 2014; Lowenstern et al., 2016; Lynne et al., 2005, 2008; Soto et al., 2019), including more recently at El Tatio (Slagter et al., 2019). In some studies, inconsistencies between radiocarbon ages and the stratigraphic position have been attributed to young/old material contaminating the samples (e.g., Lynne et al., 2008; Soto et al., 2019). Due to the rapid silicification, the mass of the residual carbon is typically minimal, and therefore, previous studies rarely presented replicate samples, $\delta^{13}C$ values, control samples with modern ages, or other observations that allow for better constraints on the determined ages.

In this study, we aim to better understand the limitations and opportunities of applying radiocarbon dating to organic material trapped in sinter using material collected from a range of depositional environments and hydrothermal features in the El Tatio geyser field. Using radiocarbon ages that we deem reliable based on stratigraphy and $\delta^{13}C$ values, our goals were to determine the longevity of activity in the geothermal field, the spatiotemporal patterns of hydrothermal discharge, and a first-order approximation of the long-term energy output. This information helps to better understand the relationships of hydrothermal activity with local deglaciation, volcanism, and heat flow in the Altiplano.

2. Materials and Methods

Sinter mounds develop independent of each other, and deposition does not typically form a continuous stratigraphic record. However, good stratigraphic records can be established within single mounds (Slagter et al., 2019). We thus selected samples from 21 different sites to obtain a representation of the present and past extent of the field and with good relative stratigraphic controls (Figure S1). Two of the samples were colocated with previously dated samples collected in the active hydrothermal area (408b, 7.22 ± 0.05 ka BP, and 429, 2.63 ± 0.02 ka BP; Slagter et al., 2019). We also collected samples from three areas that contain fresh bacterial mats (Figures S1 and S2) at temperatures of 70°C (ET540BM, 1.5 m from the vent), 50°C (ET504R, 4 m from the vent), and 40°C (ET504R, 8 m from the vent) and from one partially silicified cold marsh (ET420). We used sterilized sampling equipment to avoid contamination in those areas.

Sinter deposits are formed by precipitation of thin discontinuous layers. To account for this variability, we crushed different parts of each sample and processed replicates in separate vials of about 100 g, ending up with 70 aliquots. Following established methods for extracting organic carbon from the sinter (e.g., Howald et al., 2014; Lowenstern et al., 2016; Slagter et al., 2019), we first submerged the samples in 1 M hydrochloric acid (HCl) for 24 hr to eliminate the nonorganic carbonates. Next, we immersed the samples in concentrated (48%) hydrofluoric acid (HF) at a controlled temperature of ~70°C for 48 hr to dissolve silicate minerals. We recovered <0.4 mg of organic carbon per aliquot. Scanning electron microscopy (SEM) confirmed the existence of remnant organic material including pollen and plant remains of subaerial origin in samples from distal environments (Figure S3). Residual cyanobacteria tissue may also be present in the concentrates, but they were too small in size to be observed after the HF dissolution. Diatoms observed in microscopic analysis were completely dissolved by the HF acid digestion. We applied the same procedures to two siliciclastic marine sediment samples as known-age standards (Ortega (2014), 291 (5.99 ± 0.03 ka BP) and 369 (7.90 ± 0.03 ka BP); Table S1).

Radiocarbon samples were processed at the Keck Carbon Cycle Accelerator Mass Spectrometry Laboratory (KCCAMS) at the University of California, Irvine. Samples were combusted to CO_2 and graphitized over an iron catalyst using the hydrogen reduction method (Vogel et al., 1984). There was sufficient residual carbon to obtain ^{14}C in all aliquots and $\delta^{13}C$ for only 51 aliquots (Tables 1 and S1). For correcting the ^{14}C activity for isotopic fractionation using accelerator mass spectrometry, a standard value of $\delta^{13}C$ of −25‰ was used (Stuiver & Polach, 1977). The calibrated ages were obtained using the CALIB 7.1 code (Stuiver & Reimer, 1993) and the SHCal13 data set (Hogg et al., 2013) for the Southern Hemisphere. For the analysis, we consider an additional six samples analyzed by Slagter et al. (2019) from four sites in the active area. We divided the samples into three groups according to their depositional environment (e.g., Campbell et al., 2015): near vent (geyserite and laminated structures formed at >75°C), proximal slopes to mid-aprons (dominated by bacterial mats growing at >40°C), and distal deposits (aprons and marshes dominated by bacteria living at <40°C and plants) (Figure 2d). More details are provided in Table S1 and Figure S1.

We differentiate silica mineral phases and accessory minerals by using X-ray powder diffraction (XRPD) in the bulk samples and SEM. A few milligrams of powder from each sample were analyzed by X-ray diffraction (XRPD) using a PANalytical X'Pert Pro diffractometer equipped with a Cu X-ray tube and a fast X'Celerator detector at the University of California, Berkeley, and at the U.S. Geological Survey (USGS) in Menlo Park. We compared X-ray patterns with a database of known mineral phases using the software XPERT-PRO®.

3. Data

Calibrated ages for the sinter samples vary between modern (ET420) and 29.8 ± 0.2 ka CalBP (ET504BM) and $\delta^{13}C$ between −9.9‰ and −25.8‰ (Table 1). Modern sinter samples from bacterial mats (ET504BM, ET504R, and ET504DS) yield old apparent ages (>9.3 ka CalBP) and have the heaviest $\delta^{13}C$ (between −15.9‰ and −11.8‰). There is a linear relationship between the radiocarbon age of the sinter and water discharge temperatures where these mats develop (Figure 2b). Old/fossil sinter samples from environments dominated by bacterial mat textures (steamers and terraces Figure 2d) also have radiocarbon ages >10 ka CalBP and $\delta^{13}C$ from −16.9‰ to −9.9‰ (Figure 2c). Radiocarbon ages and $\delta^{13}C$ values of sinter samples from distal environments are highly variable (<27.3 ± 0.1 ka CalBP [ET512] and −25.8‰ to −15‰). The

Table 1
Summary of All Sinter Samples From El Tatio With Radiocarbon Ages and $\delta^{13}C$ Values Obtained in This Work and in Slagter et al. (2019)

Lab ID	Sample name	$\delta^{13}C$ (‰)	^{14}C age (ka)	±	Calib. ^{14}C age (ka CalBP)	Lab ID	Sample name	$\delta^{13}C$ (‰)	^{14}C age (ka)	±	Calib. ^{14}C age (ka CalBP)
Near vent >75°C						Distal environments <40°C					
198593	404e[a]	−25.1	9.6	0.04	10.9	227714	ET512	−21.5	22.9	0.11	27.3
198600	502b[a]	−20.5	2.2	0.02	2.2	227703	ET500	−16.1	15.0	0.05	18.2
198595	404a[a]	−24.0	5.9	0.03	6.6	228076	ET500#3	−16.3	14.8	0.05	17.9
198617	429t[a]	−22.4	2.6	0.02	2.7	191801	ET432	−19.4	14.6	0.04	17.7
198601	502m[a]	−20.4	1.7	0.02	1.5	222694	ET412	−20.5	13.2	0.03	15.8
227716	ET515#1	−15.9	16.5	0.05	19.9	222695	ET435#1	−19.4	10.6	0.03	12.5
228073	ET515#2	−19.4	16.1	0.05	19.3	222696	ET435#2	−19.1	10.3	0.03	12.0
228087	ET 515#3	−18.9	17.0	0.05	20.4	191772	ET414	−23.3	10.0	0.14	11.5
Proximal slope/mid-aprons (40–75°C)						227711	ET509#1	−23.5	9.0	0.03	10.2
227706	ET504B#1	−13.6	25.1	0.23	29.1	228094	ET509#2	−25.1	9.5	0.03	10.8
228066	ET504B#2	−13.5	30.3	0.14	34.2	227709	ET506#1	−16.2	9.1	0.03	10.2
228079	ET504B#3	−13.5	26.7	0.17	30.8	228082	ET506#3	−17.1	9.4	0.03	10.6
227708	ET504R#1	−12.7	17.9	0.06	21.6	228089	ET506#4	−17.0	9.5	0.03	10.7
228067	ET504R#2	−11.3	17.4	0.06	21.0	227712	ET510D#1	−14.3	9.0	0.03	10.7
228081	ET504R#3	−12.0	18.2	0.06	21.9	228070	ET510D#2	−16.9	8.4	0.03	9.3
227707	ET504D#1	−12.9	11.3	0.04	13.1	228085	ET510D#3	−14.6	9.1	0.03	10.2
228093	ET504D#2	−14.6	8.5	0.03	9.5	227705	ET502#1	−19.3	7.6	0.03	8.4
228080	ET504D#3	−16.0	9.5	0.03	10.6	228065	ET502#2	−20.0	7.8	0.03	8.5
227715	ET514#1	−12.4	23.6	0.12	27.7	228078	ET502#3	−19.1	7.6	0.03	8.4
228072	ET514#2	−14.1	22.6	0.10	26.9	227704	ET501#1	−25.1	7.0	0.03	7.8
228086	ET514#3	−14.6	24.7	0.12	28.7	228064	ET501#2	−25.8	7.5	0.03	8.3
227717	ET517	−15.8	22.4	0.11	26.7	228077	ET501#3	−25.6	7.6	0.03	8.4
228074	ET517#2	−16.2	21.3	0.09	25.7	191789	ET416	−21.2	4.4	0.02	4.9
228088	ET 517 #3	−16.9	20.0	0.10	24.1	191803	ET 429 A	−21.1	3.7	0.07	4.0
227713	ET510N#2	−10.5	10.3	0.03	11.9	191777	ET 429 B	−20.6	2.9	0.10	3.0
228071	ET510N#2	−9.9	11.0	0.04	12.8	191802	ET 453	−23.4	2.4	0.02	2.3
						227710	ET507#1	−22.2	2.1	0.02	2.0
						228068	ET507#2	−21.4	1.9	0.02	1.9
						228083	ET507#3	−21.3	1.9	0.02	1.8
						198614	408t[a]	−25.0	0.6	0.02	0.5
						191784	ET420	−24.0	0.0		

[a]Slagter et al. (2019).

partially silicified marsh samples (ET420) have a modern age and $\delta^{13}C$ of −24.3‰, and a distal apron sample has an age of 0.50 ± 0.02 ka CalBP and $\delta^{13}C$ of −25‰ (Slagter et al., 2019). Considering data from this study and from Slagter et al. (2019), ages from near vent environments range from 1.7 ± 0.02 ka CalBP (502 m) to 20.4 ± 0.05 ka CalBP (ET505) and the $\delta^{13}C$ values between −25.1‰ and −15.9‰ (Figure 2c). The variability of the radiocarbon ages within duplicates samples is <10%. There is no clear relationship between $\delta^{13}C$ and radiocarbon ages in duplicates.

XRPD results and microscopic analysis indicate that independent of age and stratigraphic position, opal-A is the dominant phase in all sinter samples (Figure S4). A few samples have a 2θ peak near 22°, which can be interpreted as cristobalite, opal-C, or result from an overlapping feldspar pattern. Quartz and plagioclase appear as detrital grains in lithic fragments or broken crystals, probably from surrounding volcanic rocks. The presence of lithic fragments and wide peaks supports the interpretation of opal-A plus either cristobalite or feldspar instead of opal-C.

4. Discussion

4.1. Robustness of the Data

Previous inconsistencies from radiocarbon chronologies in sinter deposits are attributed to contamination with old redeposited material (e.g., Lynne et al., 2019; Soto et al., 2019). Here, we found that modern bacterial mats are contaminated with old carbon leading to apparent radiocarbon ages of up to 30 ka and $\delta^{13}C$ values from −11‰ to −16‰ (Figures 2a and 2b). Normally, $\delta^{13}C$ in cyanobacteria varies from −20‰ to

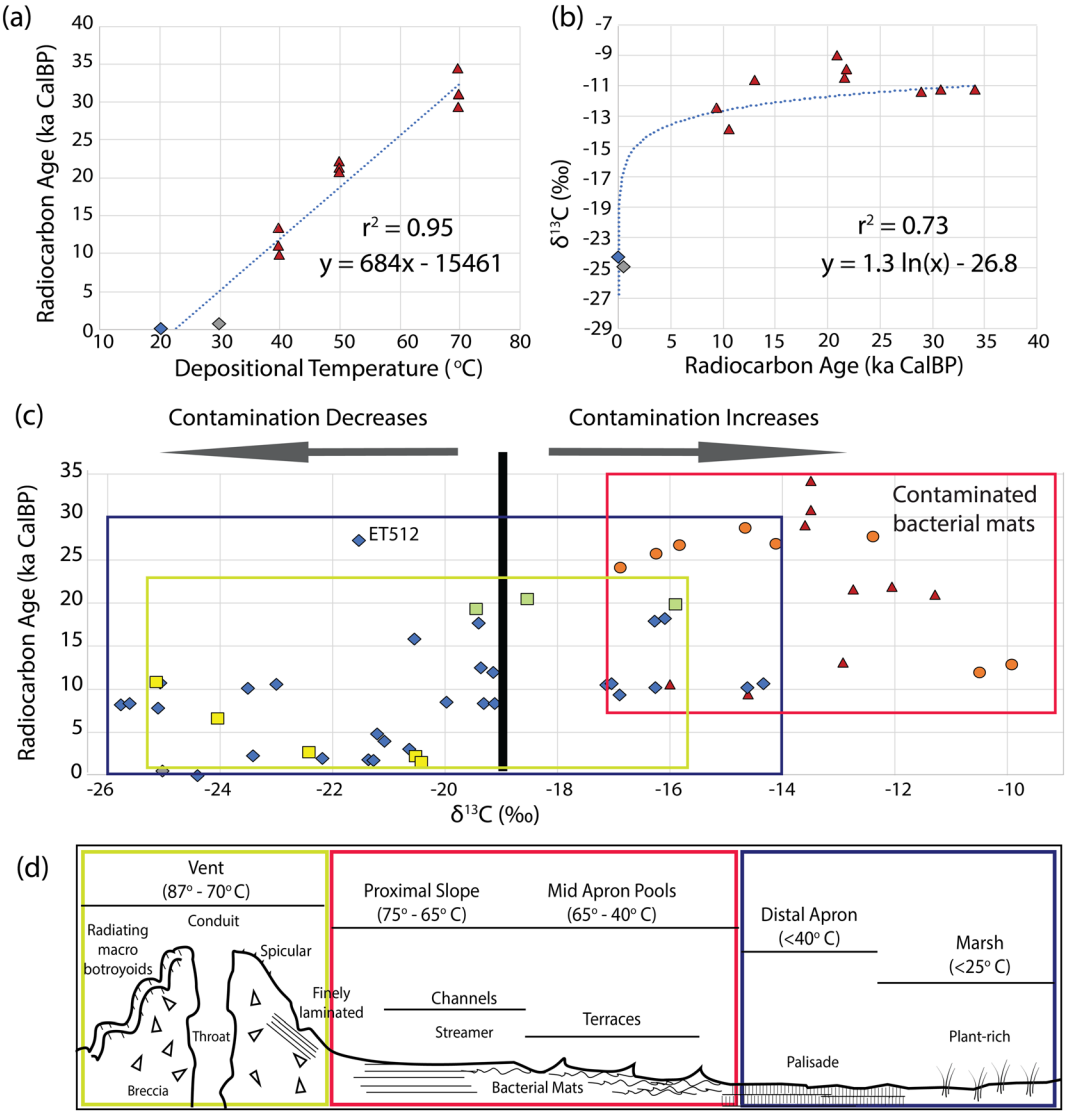

Figure 2. Age analysis according to the depositional environment. (a) Apparent ages in modern samples according to depositional temperature (linear trend). (b) Ages of modern samples showing increase with $\delta^{13}C$. Red triangles correspond to fresh bacterial mats, blue diamond to a modern partially silicified marsh, and gray diamond to a distal apron collected by Slagter et al. (2019). (c) $\delta^{13}C$ versus radiocarbon age for all sinter according to the depositional environment. Red triangles and orange circles are modern and old bacterial mats, respectively; blue diamonds are samples from distal aprons and squares from near vent environments (green are from this work and yellow from Slagter et al., 2019). (d) Depositional environment and textures summary (Campbell et al., 2015) for the samples collected in the field related to rectangles from each group in (b).

−25‰ (e.g., Jahnke et al., 2004; Popp et al., 1998; Sakata et al., 1997). Heavier $\delta^{13}C$ values found in bacterial mats in hot springs have been attributed to *Chloroflexus* and *Chloroflexus*-like organisms that metabolize and incorporate inorganic carbon (e.g., Steinke et al., 2020; Thiel et al., 2017; Van Der Meer et al., 2003). Those organisms coexist with cyanobacteria at temperatures from 60°C to 65°C in Yellowstone, USA, and Iceland (e.g., Steinke et al., 2020; Van Der Meer et al., 2007). In El Tatio, these bacteria were found in lower temperature (~40°C) bacterial mats, with $\delta^{13}C$ between −13‰ and −16‰ (Gong et al., 2020). Incorporation of inorganic carbon would yield old apparent ^{14}C ages as in magmatic environments with high CO_2 emissions (Evans et al., 2010). Even though we cannot precisely constrain the processes that give rise to the correlation between water discharge temperature and the degree of radiocarbon contamination in the modern samples (Figures 2a and 2b), data suggest that they are likely controlled by the proportion of different bacteria, metabolism in different depositional environments, or by the variable intake of carbon from different sources (dissolved inorganic carbon in water, substrate, or atmospheric carbon). Old and silicified bacterial mats

from proximal slopes to mid-aprons (red in Figures 2c and 2d) are enriched in $\delta^{13}C$ (−16‰ to −9‰), and radiocarbon ages are >10 ka. Considering the contamination observed in fresh bacterial mats identified by heavier $\delta^{13}C$ (Figures 2a and 2b), we raise a cautionary note on the apparent ^{14}C ages in those environments owing to possible contamination.

Fresh samples from distal environments dominated by plants seem to be uncontaminated and yield modern ages with $\delta^{13}C$ values of −24‰ to −25‰ (Figures 2a and 2b). A geyserite age of 2.2 ka CalBP and $\delta^{13}C$ of −20.5‰ that is coherent with the local stratigraphy (Slagter et al., 2019) suggests minimal contamination near active vents. However, older samples from near and distal environments (Figures 2c and 2d, yellow and blue) yield enriched $\delta^{13}C$ values (−16‰ and −14‰). Late Pleistocene-Holocene vegetation in the north of Chile has been documented to have $\delta^{13}C$ between −18.8‰ and −25.8‰ (e.g., Latorre et al., 2003). $\delta^{13}C$ values of cellulose in trees vary from −22‰ to −26‰ (e.g., Loader et al., 2003). Heavier $\delta^{13}C$ in old sinter samples could indicate the presence of inorganic reducing bacteria leading to older apparent ages. Changes in vent dynamics and water supply would allow bacterial mats to move up or downstream, and erosion and transport of high temperature mats can bring them to distal environments. By analyzing the field relationships among the samples, we found consistent radiocarbon ages with $\delta^{13}C$ lighter than −19‰, similar to the $\delta^{13}C$ values of vegetation in the area (e.g., Latorre et al., 2003). Thus, we set this $\delta^{13}C$ value as a threshold for assuming which radiocarbon ages reflect the actual depositional ages (Figure 2c). With this selection criterion, we discard >50% of the samples, highlighting the value of measuring $\delta^{13}C$ and selecting proper sites for interpreting radiocarbon ages in sinter.

4.2. Radiocarbon Ages

Considering only samples with reliable ages ($\delta^{13}C < -19$‰), we found that the onset of hydrothermal activity in El Tatio was in the southern part of the field, in two abandoned channels (south of current activity Figure 1). The oldest samples in this area are 27.3 ± 0.1 ka CalBP with a $\delta^{13}C$ of −21.5‰ (ET512) and 20.5 ± 0.05 ka CalBP with a $\delta^{13}C$ −19‰ (ET515). Younger radiocarbon ages in sinter have been obtained in other active systems such as Yellowstone ~8.5 ka BP (Lowenstern et al., 2016) and Steamboat, Nevada ~11.4 ka CalBP (Lynne et al., 2008). Yellowstone was ice covered until about 14 to 15 ka (Licciardi & Pierce, 2018), which probably masked any depositional record of possible hydrothermal activity.

Most Holocene ages in El Tatio are located near active vents, suggesting that the area with current hydrothermal activity has been maintained for at least ~10 ka. Late Pleistocene ages (~10 to 27 ka CalBP) appear distributed in different areas of the field, suggesting widespread hydrothermal activity during that period (Figure 1). In the north and active part of the field, the new radiocarbon ages are consistent with previously determined Holocene ages (Slagter et al., 2019) but document a longer depositional period of 17.7 ± 0.04 ka CalBP. There is a gap of 10 ka between the beginning of the hydrothermal activity in the north and the south of the field, which may either record a gap in hydrothermal activity between both areas or insufficient sampling. Fewer sinter deposits cover the west side of the field, probably because this area is younger (<4.9 ka CalBP).

4.3. Silica Phases

Previous studies of sinter in the El Tatio found opal-A to be the dominant silica phase (e.g., Fernandez-Turiel et al., 2005; Garcia-Valles et al., 2008; Jones & Renaut, 1997; Munoz-Saez et al., 2016; Nicolau et al., 2014; Rodgers et al., 2002), with opal-C found only in sinter deposits near active fumaroles (Garcia-Valles et al., 2008). Our new data indicate the absence of silica maturation even in old samples (Figure S4), consistent with proposed estimates of complete silica maturation to quartz in ~50 ka (Herdianita et al., 2000). Previous work suggested that organic material enhances silica maturation (e.g., Lynne et al., 2005, 2007); however, samples from distal aprons in El Tatio have abundant organic material without signs of maturation. The lack of mineral transformations also suggests limited postdepositional circulation of hydrothermal fluids and vent reactivation in areas with older deposits.

4.4. Implications for the Volcanic History and Heat Transport

A large magmatic body beneath the Altiplano-Puna Volcanic Complex produced large volume silicic eruptions (>15,000 km^3) between 11 and 1 Ma (De Silva, 1989; De Silva et al., 2006). During the Quaternary, large andesitic volcanoes dominated the region (De Silva et al., 1994) and several well-preserved lava domes and

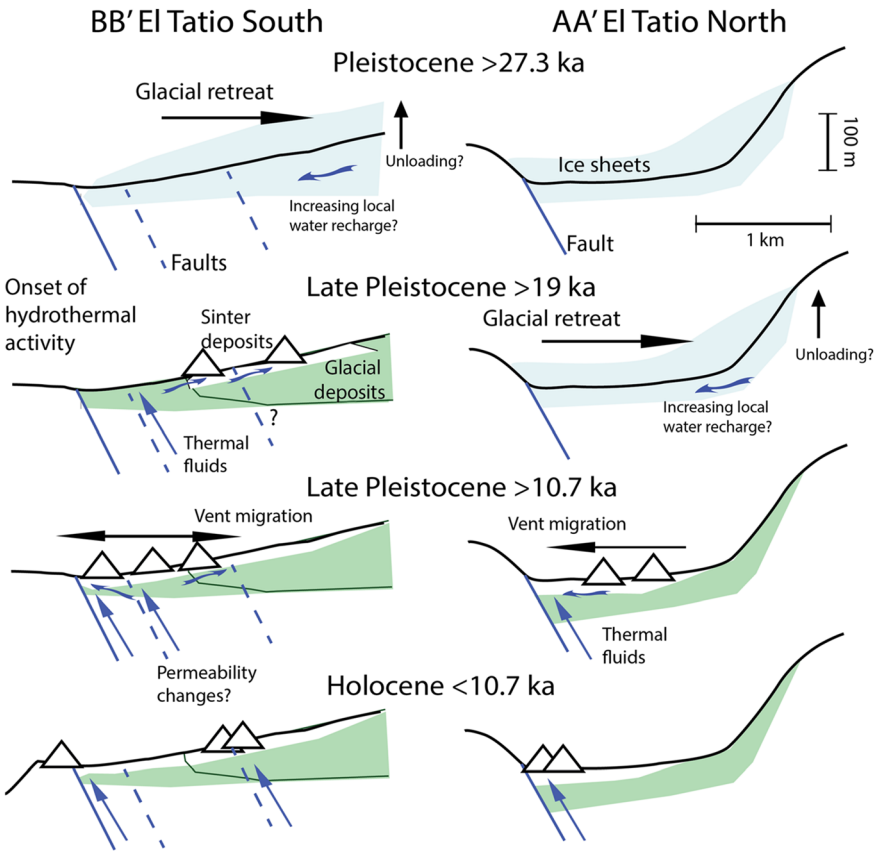

Figure 3. Schematic profiles showing the evolution of the El Tatio from the late Pleistocene to the present for the southern and northern areas (BB′ and AA′ in Figure 1). The background line shows the topography with a 5× vertical exaggeration. The blue polygon indicates ice, green glacial deposit, and white sinter. Thicknesses of ice and deposits are schematic and not scaled.

volcanic cones are inferred to be of Pleistocene to Holocene age based on stratigraphic relationships with glacial deposits (e.g., De Silva et al., 1994; González-Ferrán, 1995; Marinovic & Lahsen, 1984). The lack of volcanic deposits intercalated between sinter indicates that El Tatio has not been affected by volcanic eruptions since at least ~27 ka. The products of the few Holocene eruptions in the area, including from Putana Volcano (~32 km toward the SE), San Pedro Volcano (~60 km toward the NW), and Lascar (~120 km to the S), (Global Volcanism Program, 2013), have not reached El Tatio.

The intense and prolonged hydrothermal activity requires a cooling magmatic heat source. The amount of heat released over time constrains the size of the magmatic source. The current estimated advective heat flow from El Tatio thermal discharge is 120–170 MW (Munoz-Saez et al., 2018). Assuming a similar value for the last 20 ka, as a first-order approximation, we estimate that $Q_T \sim 10^{14}$ MJ has been advected by the hydrothermal system. We estimate an equivalent volume of cooled magma of ~4×10^{10} m^3, considering $Q_T = V\rho(\Delta T C_p + \Delta h)$, a combination of sensible and latent heat, with C_p the heat capacity (~1.4 kJ/kgK), Δh the specific heat of fusion (~350 kJ/kg), ρ the density (~2,400 kg/m^3) of magma (Lesher & Spera, 2015), and ΔT the temperature difference between the magma and geothermal reservoir (~500°C).

4.5. Implications for the Glacial History

Owing to the current aridity of the northern Chilean Andes, glaciers are absent on the highest mountains (e.g., Clapperton et al., 1997), and this dryness has been persistent for the last 12 Ma (e.g., Jordan et al., 2014). However, humid periods during the Pleistocene and Holocene enabled glaciation in the Altiplano (e.g., Ammann et al., 2001; Kull & Grosjean, 2000; Rodbell et al., 2009). Cosmogenic nuclide exposure dating of moraines in the Peruvian-Bolivian Altiplano indicate that the greatest glacial extent during the Local

Glacial Maximum (LGM) was prior to 26 ka (Luna et al., 2018; Smith et al., 2005; Zech et al., 2009). However, moraine chronologies in the Argentinean-Bolivian Altiplano (e.g., Blard et al., 2009, 2014; Zech et al., 2009) indicate late readvances, synchronous with a regional humid period (Tauca Period 17–15 ka, Sylvestre et al., 1999; Placzek et al., 2006). Deglaciation on the Chilean Altiplano is largely undocumented, and exposure ages on moraines near El Tatio show large variability due to inheritance from rock exposure prior to glaciation (Ward et al., 2015, 2017).

At El Tatio, the lack of glacial deposits covering sinter, the absence of cryogenic textures, and the vegetation trapped in the sinter suggest that hydrothermal activity occurred in absence of ice cover. Old radiocarbon ages in the south of the field (ET512 and ET515) overlay the rim of a large glacial moraine (Figure 1). The oldest radiocarbon age of 27.3 ka CalBP (ET512) is consistent with exposure ages (^{10}Be) between 24.6 and 30.7 ka measured ~14 km south of El Tatio (La Torta Valley, Ward et al., 2015). The oldest hydrothermal deposit in the north of the field (17.7 ka CalBP, ET432) agrees with ^{36}Cl exposure ages >20 ka in moraines ~5 km north of El Tatio (Ward et al., 2017). At elevations >4,800 m to ~100 km east of El Tatio (Uturuncu Volcano), moraine ages >14 ka (Blard et al., 2014) also indicate later glacial readvances affecting higher elevations toward the western part of the Altiplano (Ward et al., 2015).

A temporal correlation of the onset of surficial hydrothermal activity with glacial–interglacial cyclicity is suggested by the correspondence of the oldest ^{14}C ages (Figure 1, ET512, ET515, and ET432) and the few cosmogenic exposure ages in nearby moraines (Ward et al., 2015, 2017). In the south of the field, the onset of hydrothermal activity at ~27 ka followed the deglaciation from the early LGM (Figure 3). In the north, hydrothermal activity initiated after ~18 ka, probably due to extended glacial coverage until the late LGM in higher elevations. Between ~18 and ~10.7 ka, hydrothermal activity was probably widespread across the entire field. Since the beginning of Holocene, large sinter mounds and geysers were concentrated in the current location of hydrothermal activity.

5. Conclusions

Radiocarbon ages of organic material trapped in sinter deposits along with δ^{13}C values provide valuable information about possible sources of carbon contamination and the reliability of reported ages. In El Tatio, bacterial mats living at temperatures of 40°C to 75°C can use inorganic carbon resulting in apparently old radiocarbon ages and heavy δ^{13}C values (>−16‰). For our interpretations of postglacial hydrothermal activity, we considered only samples from environments without bacterial mats and with δ^{13}C values < −19‰. Because nearly all sinter deposits consist mainly of opal-A, the silica mineral phases were not useful for determining relative sinter ages. Our data indicate that El Tatio is a long-lived hydrothermal system that has been active since ~27 ka CalBP. The spatial and temporal distribution of pre-Holocene sinter ages suggests widespread hydrothermal activity in the field. The current spatial distribution of thermal features has been maintained around the main tectonic structures since the early Holocene. The oldest sinter ages imply that the most recent volcanic activity in the vicinity of El Tatio was >27 ka. Given the inferred longevity of hydrothermal activity, our order-of-magnitude estimate for thermal discharge during the Holocene (~10^{14} MJ) requires a large body of cooling magma. The oldest radiocarbon ages in sinter are consistent with moraine chronologies in the area and suggest that hydrothermal activity began shortly after glacier retreat. Our results illustrate that sinter deposits are rich geological archives and provide useful records that can be applied in other areas of the Altiplano.

Acknowledgments

This research was supported by the National Science Foundation (EAR1724986), Fondo de Fomento al Desarrollo Científico y Tecnológico (FONDEF) Project 15090013 "Centro de Excelencia en Geotermia de Los Andes," CEGA, and FONDECYT Postdoctoral Grant (Comisión Nacional de Investigación Científica y Tecnológica, 3170007). Additional support was provided by ICM grant "Millennium Nucleus for Metal Tracing Along Subduction." Shaul Hurwitz and David Damby were funded by the USGS Volcano Hazards Program and Geothermal Energy Project. We thank J. R. Skok and Jian Gong who provided essential help in the field; Cristina Ortega for the samples used as standards; John Southon from the Keck Carbon Cycle AMS Laboratory for the radiocarbon measurements; Veronica Rodriguez for helping with lab procedures; Michael Kaplan for discussions; and two anonymous reviewers, Andrew Cyr and Michael Clynne, for their constructive comments. Fieldwork was performed with the permission of the Aymara Communities of Caspana and Toconce. Any use of trade, firm, or product names is for descriptive purposes and does not imply endorsement by the U.S. Government. All data collected for this paper (Table S1) has been submitted to the PANGAEA repository archives (at https://doi.org/10.1594/PANGAEA.914480).

References

Ammann, C., Jenny, B., Kammer, K., & Messerli, B. (2001). Late Quaternary glacier response to humidity changes in the arid Andes of Chile (18–29°S). *Palaeogeography, Palaeoclimatology, Palaeoecology*, *172*(3-4), 313–326. https://doi.org/10.1016/S0031-0182(01)00306-6

Blard, P. H., Lavé, J., Farley, K. A., Fornari, M., Jiménez, N., & Ramirez, V. (2009). Late local glacial maximum in the Central Altiplano triggered by cold and locally-wet conditions during the paleolake Tauca episode (17–15 ka, Heinrich 1). *Quaternary Science Reviews*, *28*(27–28), 3414–3427. https://doi.org/10.1016/j.quascirev.2009.09.025

Blard, P. H., Lave, J., Farley, K. A., Ramirez, V., Jimenez, N., Martin, L. C., et al. (2014). Progressive glacial retreat in the Southern Altiplano (Uturuncu volcano, 22°S) between 65 and 14 ka constrained by cosmogenic ^{3}He dating. *Quaternary Research*, *82*(1), 209–221. https://doi.org/10.1016/j.yqres.2014.02.002

Campbell, K. A., Buddle, T. F., & Browne, P. R. L. (2003). Late Pleistocene siliceous sinter associated with fluvial, lacustrine, volcaniclastic and landslide deposits at Tahunaatara, Taupo Volcanic Zone, New Zealand. *Earth and Environmental Science Transactions of the Royal Society of Edinburgh*, *94*(4), 485–501. https://doi.org/10.1017/S0263593300000833

Campbell, K. A., Guido, D. M., Gautret, P., Foucher, F., Ramboz, C., & Westall, F. (2015). Geyserite in hot-spring siliceous sinter: Window on Earth's hottest terrestrial (paleo) environment and its extreme life. *Earth-Science Reviews*, *148*, 44–64. https://doi.org/10.1016/j.earscirev.2015.05.009

Clapperton, C. M., Clayton, J. D., Benn, D. I., Marden, C. J., & Argollo, J. (1997). Late Quaternary glacier advances and palaeolake high-stands in the Bolivian Altiplano. *Quaternary International*, *38*, 49–59. https://doi.org/10.1016/s1040-6182(96)00020-1

De Silva, S., Zandt, G., Trumbull, R., Viramonte, J. G., Salas, G., & Jiménez, N. (2006). Large ignimbrite eruptions and volcano-tectonic depressions in the Central Andes: A thermomechanical perspective. *Geological Society, London, Special Publications*, *269*(1), 47–63. https://doi.org/10.1144/GSL.SP.2006.269.01.04

De Silva, S. L. (1989). Altiplano-Puna volcanic complex of the central Andes. *Geology*, *17*(12), 1102–1106. https://doi.org/10.1130/0091-7613(1989)017<1102:APVCOT>2.3.CO;2

De Silva, S. L., Self, S., Francis, P. W., Drake, R. E., & Carlos, R. R. (1994). Effusive silicic volcanism in the Central Andes: The Chao dacite and other young lavas of the Altiplano-Puna Volcanic Complex. *Journal of Geophysical Research: Solid Earth*, *99*(B9), 17,805–17,825. https://doi.org/10.1029/94JB00652

Drake, B. D., Campbell, K. A., Rowland, J. V., Guido, D. M., Browne, P. R., & Rae, A. (2014). Evolution of a dynamic paleo-hydrothermal system at Mangatete, Taupo Volcanic Zone, New Zealand. *Journal of Volcanology and Geothermal Research*, *282*, 19–35. https://doi.org/10.1016/j.jvolgeores.2014.06.010

Evans, W. C., Bergfeld, D., McGeehin, J. P., King, J. C., & Heasler, H. (2010). Tree-ring ^{14}C links seismic swarm to CO_2 spike at Yellowstone, USA. *Geology*, *38*(12), 1075–1078. https://doi.org/10.1130/G31345.1

Fernandez-Turiel, J. L., Garcia-Valles, M., Gimeno-Torrente, D., Saavedra-Alonso, J., & Martinez-Manent, S. (2005). The hot spring and geyser sinters of El Tatio, Northern Chile. *Sedimentary Geology*, *180*(3–4), 125–147. https://doi.org/10.1016/j.sedgeo.2005.07.005

Fournier, R. O. (1977). Chemical geothermometers and mixing models for geothermal systems. *Geothermics*, *5*(1-4), 41–50. https://doi.org/10.1016/0375-6505(77)90007-4

Garcia-Valles, M., Fernandez-Turiel, J. L., Gimeno-Torrente, D., Saavedra-Alonso, J., & Martinez-Manent, S. (2008). Mineralogical characterization of silica sinters from the El Tatio geothermal field, Chile. *American Mineralogist*, *93*(8–9), 1373–1383. https://doi.org/10.2138/am.2008.2583

Giggenbach, W. F. (1988). Geothermal solute equilibria. Derivation of Na-K-Mg-Ca geoindicators. *Geochimica et Cosmochimica Acta*, *52*(12), 2749–2765. https://doi.org/10.1016/0016-7037(88)90143-3

Global Volcanism Program, (2013). *Volcanoes of the world*, v. 4.8.2. E. Venzke (ed.). Washington DC: Smithsonian Institution. Downloaded 22 Aug 2019. https://doi.org/10.5479/si.GVP.VOTW4-2013

Gong, J., Myers, K. D., Munoz-Saez, C., Homann, M., Rouillard, J., Wirth R., et al. (2020). Formation and Preservation of Microbial Palisade Fabric in Silica Deposits from El Tatio, Chile. *Astrobiology*, *20*(4), 500–524. http://doi.org/10.1089/ast.2019.2025

González-Ferrán, O. (1995). Volcanes de Chile. Santiago, Chile: Instituto Geográfico Militar.

Herdianita, N. R., Browne, P. R. L., Rodgers, K. A., & Campbell, K. A. (2000). Mineralogical and textural changes accompanying ageing of silica sinter. *Mineralium Deposita*, *35*(1), 48–62. https://doi.org/10.1007/s001260050005

Hogg, A. G., Hua, Q., Blackwell, P. G., Niu, M., Buck, C. E., Guilderson, T. P., et al. (2013). SHCal13 Southern Hemisphere calibration, 0–50,000 years cal BP. *Radiocarbon*, *55*(4), 1889–1903. https://doi.org/10.2458/azu_js_rc.55.16783

Howald, T., Person, M., Campbell, A., Lueth, V., Hofstra, A., Sweetkind, D., et al. (2014). Evidence for long timescale (>103 years) changes in hydrothermal activity induced by seismic events. *Geofluids*, *15*(1–2), 252–268.

Jahnke, L. L., Embaye, T., Hope, J., Turk, K. A., Van Zuilen, M., Des Marais, D. J., et al. (2004). Lipid biomarker and carbon isotopic signatures for stromatolite-forming, microbial mat communities and *Phormidium* cultures from Yellowstone National Park. *Geobiology*, *2*(1), 31–47. https://doi.org/10.1111/j.1472-4677.2004.00021.x

Jones, B., & Renaut, R. W. (1997). Formation of silica oncoids around geysers and hot springs at El Tatio, northern Chile. *Sedimentology*, *44*(2), 287–304. https://doi.org/10.1111/j.1365-3091.1997.tb01525.x

Jones, B., & Renaut, R. W. (2003). Hot spring and geyser sinters: The integrated product of precipitation, replacement, and deposition. *Canadian Journal of Earth Sciences*, *40*(11), 1549–1569. https://doi.org/10.1139/e03-078

Jordan, T. E., Kirk-Lawlor, N. E., Blanco, N. P., Rech, J. A., & Cosentino, N. J. (2014). Landscape modification in response to repeated onset of hyperarid paleoclimate states since 14 Ma, Atacama Desert, Chile. *GSA Bulletin*, *126*(7–8), 1016–1046. https://doi.org/10.1130/B30978.1

Konhauser, K. O., Jones, B., Reysenbach, A. L., & Renaut, R. W. (2003). Hot spring sinters: Keys to understanding Earth's earliest life forms. *Canadian Journal of Earth Sciences*, *40*(11), 1713–1724. https://doi.org/10.1139/e03-059

Kull, C., & Grosjean, M. (2000). Late Pleistocene climate conditions in the north Chilean Andes drawn from a climate–glacier model. *Journal of Glaciology*, *46*(155), 622–632. https://doi.org/10.3189/172756500781832611

Lahsen, A. (1976). La actividad geotermal y sus relaciones con la tectónica y el volcanismo en el norte de Chile, I Congreso Geológico Chileno, Actas, B105 – B127, Antofagasta.

Latorre, C., Betancourt, J. L., Rylander, K. A., Quade, J., & Matthei, O. (2003). A vegetation history from the arid prepuna of northern Chile (22–23°S) over the last 13 500 years. *Palaeogeography, Palaeoclimatology, Palaeoecology*, *194*(1–3), 223–246. https://doi.org/10.1016/S0031-0182(03)00279-7

Lesher, C. E., & Spera, F. J. (2015). Thermodynamic and transport properties of silicate melts and magma. In *The encyclopedia of volcanoes*, (pp. 113–141). Cambridge, Massachusetts, USA: Elsevier, Academic press.

Licciardi, J. M., & Pierce, K. L. (2018). History and dynamics of the Greater Yellowstone Glacial System during the last two glaciations. *Quaternary Science Reviews*, *200*, 1–33. https://doi.org/10.1016/j.quascirev.2018.08.027

Loader, N. J., Robertson, I., & McCarroll, D. (2003). Comparison of stable carbon isotope ratios in the whole wood, cellulose and lignin of oak tree-rings. *Palaeogeography, Palaeoclimatology, Palaeoecology*, *196*(3–4), 395–407. https://doi.org/10.1016/S0031-0182(03)00466-8

Lowenstern, J. B., Hurwitz, S., & McGeehin, J. P. (2016). Radiocarbon dating of silica sinter deposits in shallow drill cores from the Upper Geyser Basin, Yellowstone National Park. *Journal of Volcanology and Geothermal Research*, *310*, 132–136. https://doi.org/10.1016/j.jvolgeores.2015.12.005

Luna, L. V., Bookhagen, B., Niedermann, S., Rugel, G., Scharf, A., & Merchel, S. (2018). Glacial chronology and production rate cross-calibration of five cosmogenic nuclide and mineral systems from the southern Central Andean Plateau. *Earth and Planetary Science Letters*, *500*, 242–253. https://doi.org/10.1016/j.epsl.2018.07.034

Lynne, B. Y., Campbell, K. A., James, B. J., Browne, P. R., & Moore, J. (2007). Tracking crystallinity in siliceous hot-spring deposits. *American Journal of Science*, *307*(3), 612–641. https://doi.org/10.2475/03.2007.03

Lynne, B. Y., Campbell, K. A., Moore, J., & Browne, P. R. L. (2005). Diagenesis of 1900-year-old siliceous sinter (opal-A to quartz) at Opal Mound, Roosevelt Hot Springs, Utah, U.S.A. *Sedimentary Geology*, *119*, 249–278.

Lynne, B. Y., Campbell, K. A., Moore, J. N., & Browne, P. R. L. (2008). Origin and evolution of the Steamboat Springs siliceous sinter deposit, Nevada, U.S.A. *Sedimentary Geology*, *210*(3-4), 111–131. https://doi.org/10.1016/j.sedgeo.2008.07.006

Marinovic, N., Lahsen, A. (1984). Hoja Calama: región de Antofagasta: carta geológica de Chile 1: 250.000. Servicio Nacional de Geología y Minería, Chile.

Munoz-Saez, C., Manga, M., & Hurwitz, S. (2018). Hydrothermal discharge from the El Tatio basin, Atacama, Chile. *Journal of Volcanology and Geothermal Research*, *361*, 25–35. https://doi.org/10.1016/j.jvolgeores.2018.07.007

Munoz-Saez, C., Saltiel, S., Manga, M., Nguyen, C., & Gonnermann, H. (2016). Physical and hydraulic properties of modern sinter deposits: El Tatio, Atacama. *Journal of Volcanology and Geothermal Research*, *325*, 156–168. https://doi.org/10.1016/j.jvolgeores.2016.06.026

Nicolau, C., Reich, M., & Lynne, B. (2014). Physico-chemical and environmental controls on siliceous sinter formation at the high-altitude El Tatio geothermal field, Chile. *Journal of Volcanology and Geothermal Research*, *282*, 60–76. https://doi.org/10.1016/j.jvolgeores.2014.06.012

Ortega, C. (2014). Variabilidad climática en la costa semiárida de Chile (30°-32°S) durante los últimos 13.000 años. Available at: http://repositorio.uchile.cl/handle/2250/130327

Placzek, C., Quade, J., & Patchett, P. J. (2006). Geochronology and stratigraphy of late Pleistocene lake cycles on the southern Bolivian Altiplano: Implications for causes of tropical climate change. *Geological Society of America Bulletin*, *118*(5–6), 515–532. https://doi.org/10.1130/B25770.1

Popp, B. N., Laws, E. A., Bidigare, R. R., Dore, J. E., Hanson, K. L., & Wakeham, S. G. (1998). Effect of phytoplankton cell geometry on carbon isotopic fractionation. *Geochimica et Cosmochimica Acta*, *62*(1), 69–77. https://doi.org/10.1016/S0016-7037(97)00333-5

Rodbell, D. T., Smith, J. A., & Mark, B. G. (2009). Glaciation in the Andes during the Lateglacial and Holocene. *Quaternary Science Reviews*, *28*(21-22), 2165–2212. https://doi.org/10.1016/j.quascirev.2009.03.012

Rodgers, K. A., Browne, P. R. L., Buddle, T. F., Cook, K. L., Greatrex, R. A., Hampton, W. A., et al. (2004). Silica phases in sinters and residues from geothermal fields of New Zealand. *Earth-Science Reviews*, *66*(1–2), 1–61. https://doi.org/10.1016/j.earscirev.2003.10.001

Rodgers, K. A., Greatrex, R., Hyland, M., Simmons, S. F., & Browne, P. R. L. (2002). A modern, evaporitic occurrence of teruggite, $Ca_4MgB_{12}As_2O_{28}{\cdot}18H_2O$, and nobleite, $CaB_6O_{10}{\cdot}4H_2O$, from the El Tatio geothermal field, Antofagasta Province, Chile. *Mineralogical Magazine*, *66*(2), 253–259. https://doi.org/10.1180/0026461026620026

Sakata, S., Hayes, J. M., McTaggart, A. R., Evans, R. A., Leckrone, K. J., & Togasaki, R. K. (1997). Carbon isotopic fractionation associated with lipid biosynthesis by a cyanobacterium: Relevance for interpretation of biomarker records. *Geochimica et Cosmochimica Acta*, *61*(24), 5379–5389. https://doi.org/10.1016/S0016-7037(97)00314-1

Salisbury, M. J., Jicha, B. R., de Silva, S. L., Singer, B. S., Jiménez, N. C., & Ort, M. H. (2011). $^{40}Ar/^{39}Ar$ chronostratigraphy of Altiplano-Puna volcanic complex ignimbrites reveals the development of a major magmatic province. *Geological Society of America Bulletin*, *123*(5-6), 821–840. https://doi.org/10.1130/B30280.1

Slagter, S., Reich, M., Munoz-Saez, C., Southon, J., Morata, D., Barra, F., et al. (2019). Environmental controls on silica sinter formation revealed by radiocarbon dating. *Geology*, *47*(4), 330–334. https://doi.org/10.1130/G45859.1

Smith, J. A., Seltzer, G. O., Farber, D. L., Rodbell, D. T., & Finkel, R. C. (2005). Early local last glacial maximum in the tropical Andes. *Science*, *308*(5722), 678–681. https://doi.org/10.1126/science.1107075

Soto, M. F., Hochstein, M. P., Campbell, K., & Keys, H. (2019). Sporadic and waning hot spring activity in the Tokaanu Domain, Hipaua-Waihi-Tokaanu geothermal field, Taupo Volcanic Zone, New Zealand. *Geothermics*, *77*, 288–303. https://doi.org/10.1016/j.geothermics.2018.10.005

Steinke, L., Slysz, G. W., Lipton, M. S., Klatt, C., Moran, J. J., Romine, M. F., et al. (2020). Short-term stable isotope probing of proteins reveals taxa incorporating inorganic carbon in a hot spring microbial mat. *Applied and Environmental Microbiology*, *86*(7). https://doi.org/10.1128/AEM.01829-19

Stuiver, M., & Polach, H. A. (1977). Reporting of C-14 data—Discussion. *Radiocarbon*, *19*(3), 355–363. https://doi.org/10.1017/S0033822200003672

Stuiver, M., & Reimer, P. J. (1993). Extended ^{14}C database and revised CALIB radiocarbon calibration program. *Radiocarbon*, *35*(1), 215–230. https://doi.org/10.1017/S0033822200013904

Sylvestre, F., Servant, M., Servant-Vildary, S., Causse, C., Fournier, M., & Ybert, J. P. (1999). Lake-level chronology on the Southern Bolivian Altiplano (18–23°S) during late glacial time and the early Holocene. *Quaternary Research*, *51*(1), 54–66. https://doi.org/10.1006/qres.1998.2017

Thiel, V., Hügler, M., Ward, D. M., & Bryant, D. A. (2017). The dark side of the mushroom spring microbial mat: Life in the shadow of chlorophototrophs. II. Metabolic functions of abundant community members predicted from metagenomic analyses. *Frontiers in Microbiology*, *8*, 943. https://doi.org/10.3389/fmicb.2017.00943

Van der Meer, M. T., Schouten, S., Damsté, J. S. S., de Leeuw, J. W., & Ward, D. M. (2003). Compound-specific isotopic fractionation patterns suggest different carbon metabolisms among *Chloroflexus*-like bacteria in hot-spring microbial mats. *Applied and Environmental Microbiology*, *69*(10), 6000–6006. https://doi.org/10.1128/AEM.69.10.6000-6006.2003

Van Der Meer, M. T., Schouten, S., Damsté, J. S. S., & Ward, D. M. (2007). Impact of carbon metabolism on ^{13}C signatures of cyanobacteria and green non-sulfur-like bacteria inhabiting a microbial mat from an alkaline siliceous hot spring in Yellowstone National Park (USA). *Environmental Microbiology*, *9*(2), 482–491. https://doi.org/10.1111/j.1462-2920.2006.01165.x

Vogel, J. S., Southon, J. R., Nelson, D. E., & Brown, T. A. (1984). Performance of catalytically condensed carbon for use in accelerator mass spectrometry. *Nuclear Instruments and Methods in Physics Research Section B: Beam Interactions with Materials and Atoms*, *5*(2), 289–293. https://doi.org/10.1016/0168-583X(84)90529-9

Ward, D., Thornton, R., & Cesta, J. (2017). Across the Arid Diagonal: Deglaciation of the western Andean Cordillera in southwest Bolivia and northern Chile. *Cuadernos de investigación geográfica/Geographical Research Letters*, *43*(2), 667–696. https://doi.org/10.18172/cig.3209

Ward, D. J., Cesta, J. M., Galewsky, J., & Sagredo, E. (2015). Late Pleistocene glaciations of the arid subtropical Andes and new results from the Chajnantor Plateau, northern Chile. *Quaternary Science Reviews*, *128*, 98–116. https://doi.org/10.1016/j.quascirev.2015.09.022

Zech, J., Zech, R., Kubik, P. W., & Veit, H. (2009). Glacier and climate reconstruction at Tres Lagunas, NW Argentina, based on ^{10}Be surface exposure dating and lake sediment analyses. *Palaeogeography, Palaeoclimatology, Palaeoecology*, *284*(3-4), 180–190. https://doi.org/10.1016/j.palaeo.2009.09.023